Vertical integration of self-rolled-up microtube and silicon waveguides: a two-channel optical add–drop multiplexer

Setareh Sedaghat and Abbas Zarifkar*

Department of Communications and Electronics, School of Electrical and Computer Engineering, Shiraz University, Shiraz, Iran

**Corresponding author: zarifkar@shirazu.ac.ir*

Received October 20, 2016; accepted December 2, 2016; posted online December 30, 2016

A novel design of a two-channel optical add–drop multiplexer based on a self-rolled-up microtube (SRM) is presented. This design consists of an SRM that has a parabolic lobe-like pattern along the tube's axial direction, as well as straight silicon waveguides and a 180° waveguide bend. The vertical configuration of the SRM and waveguides is analyzed by the coupled mode theory for achieving the optimum gap. In the critical coupling regime, when the device serves as an optical demultiplexer, the minimum insertion loss is 1.94 dB, and the maximum channel crosstalk is −6.036 dB. Also, as an optical multiplexer, the maximum crosstalk becomes −11.9 dB.

OCIS codes: 250.5300, 230.0230, 230.3990, 230.5750.
doi: 10.3788/COL201715.022501.

Rapid evolution of the chip-level interconnect technologies enables us to design low-power-consuming and compact components. In order to boost bandwidth density and select and route dense wavelength-division multiplexing (DWDM) signals for high bit-rate transmission, an optical add–drop multiplexer (OADM) as one of the interconnect devices has been introduced. Various technologies such as fiber Bragg gratings[1], arrayed waveguide gratings[2], cascaded Mach–Zehnder (MZ) interferometers[3], and microring resonators (MRRs)[4] have been used for OADMs. The main drawback of OADMs based on fiber Bragg grating and arrayed waveguide grating is their large sizes, which makes them unsuitable for integrated circuits. Furthermore, the performance of an MZ-based OADM is severely dependent on the fabrication process, which may degrade the characteristics of the device, such as insertion loss and crosstalk level. For MRR-based OADMs, different configurations of MRRs have been proposed[4,5]. However, in these schemes, increasing the add–drop wavelengths needs more MRRs, which causes degradation of the performance, multi-functionality, and reliability of the device due to an increase in inter-chip interconnects.

Three-dimensional (3D) integrated systems can be utilized to minimize the interconnect length and eliminate speed-limiting chip interconnects[6]. A self-rolled-up microtube (SRM), as a novel microresonator, was introduced in the middle 2000s[7,8]. The rolling mechanism for the fabrication of the tubular shape of this structure facilitates the achievement of 3D light confinement in azimuthal, radial, and axial directions[9,10]. Furthermore, several experimental reports on the vertical coupling of this structure and other waveguides, both manually and monolithically, have been presented[11,12]. To the best of our knowledge, there has been no research conducted on designing passive SRM-based optoelectronic devices, particularly on an OADM, so far.

In this Letter, a new scheme of two-channel OADMs based on the vertical integration of the SRM and waveguides is proposed and analyzed. The components are designed, and the operating principle of the structure and performance of the designed two-channel OADM are investigated. It is shown that this scheme has the potential to add and/or drop several wavelengths simultaneously.

The layout of the vertical configuration for a two-channel OADM is shown in Fig. 1. As can be seen, this device is composed of an SRM with a parabolic lobe-like pattern along the axial direction, which is coupled to the waveguides embedded in two vertically aligned substrates. In the following, we will design the device components, including the straight waveguides, 180° waveguide bend, and SRM.

A straight waveguide and a 180° waveguide bend are exploited as the components of our proposed scheme for

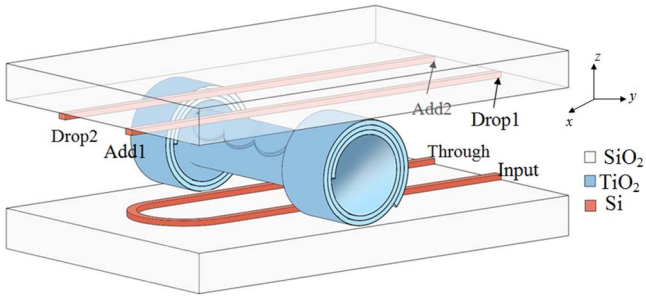

Fig. 1. Layout of the vertical two-channel OADM based on the SRM, which is composed of an SRM with a parabolic lobe-like pattern along the axial direction, a 180° silicon waveguide bend, and a silicon straight waveguides in two vertical aligned substrates.

the two-channel SRM-based OADM, as shown in Fig. 1. Since the bending loss is inherent to the waveguide bend, while a single-mode transmission at the wavelength of 1.55 μm is essential for this photonic integrated circuit, designing low-loss and single-mode waveguides is of vital importance.

The device is fabricated on SiO_2 layers. The thickness of the SiO_2 layers is 4 μm, and the top silicon layers are 215.5 nm thick. Figure 2 shows that for a given 215.5-nm-thick silicon waveguide, a large range of effective indices from 1.8 to 2.8 can be achieved, corresponding to the propagation constants of the TE_0 and TE_1 modes at $\lambda = 1.55$ μm. Also, it can be seen that the width of the silicon waveguides for a single-mode transmission is limited up to 0.7 μm. Therefore, the silicon waveguides having cross sections of 400 nm × 215.5 nm are chosen to meet the single-mode transmission condition.

For the bent section, the bending radius is set to 4.5 μm. In order to reduce the transition loss between the straight waveguide and the bent waveguide, a lateral offset is considered between these two sections. A top view of a 180° waveguide bend with a shift in the lateral direction is illustrated in Fig. 3(a). Figure 3(b) shows the 180° bending loss (including both radiation and transition losses) as a function of the lateral offset for a silicon waveguide having the same cross section as the straight waveguides with the bending radius of 4.5 μm at a wavelength of 1.55 μm. As can be seen, the optimum lateral offset is 10 nm, where the minimum of the total bending loss (~0.02753 dB) occurs. Although the lateral offset partly reduces the transition loss between the straight and bent parts of the waveguide[13], the radiation loss causes an increasing trend, as shown in Fig. 3(b).

The SRM is introduced as a key component for the proposed two-channel OADM. As illustrated in Fig. 1, the SRM includes three parts: one free-standing part and two legs. The central part is thinner and has no contact with the substrate, while the thicker legs remain in touch. Therefore, the free-standing part of SRM acts as a resonator because of the refractive index contrast between the strained layers and the surrounding region. The non-scaled cross section of the free-standing part of this SRM is shown in Fig. 4(a). In this design, a titanium dioxide (TiO_2) SRM with an 8 μm radius and three windings in the free-standing part is utilized, which result in the wall thickness of 345 nm. The parameters are tailored such that the effective index of the SRM matches the effective index of the single-mode silicon waveguides ($n_{\text{eff}} = 2.088$ at $\lambda = 1.55$ μm). The reasons for choosing TiO_2 for this SRM are its high refractive index ($n \geq 2.1$), complementary metal-oxide-semiconductor (CMOS) compatibility, and transparency for both visible and telecom wavelengths[14,15]. Although the void in the SRM wall can degrade the quality (Q) -factor[8,16], the experimental report shows that the SRM wall thickness has a more severe effect than the void on the Q-factor for telecommunication wavelengths[11].

Because of the rolling mechanism of TiO_2 strained bilayers, the broken rotational symmetry between the inner and outer edges of the SRM introduces an asymmetric parameter (γ) [as presented in Fig. 4(a)] that affects the resonant wavelengths, which resulted from the light confinement in the axial direction and cross-section plane[17–19]. Figure 4(b) shows the resonant wavelengths of the designed SRM versus γ for the 65th azimuthal mode and the first radial mode. As can be seen, increasing the asymmetric parameter from 0 to 2π increases the optical path

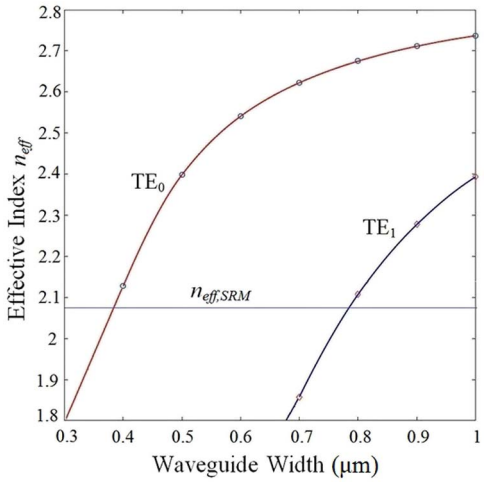

Fig. 2. Effective index of the optical modes in 215.5-nm-thick silicon waveguide for different widths at $\lambda = 1.55$ μm.

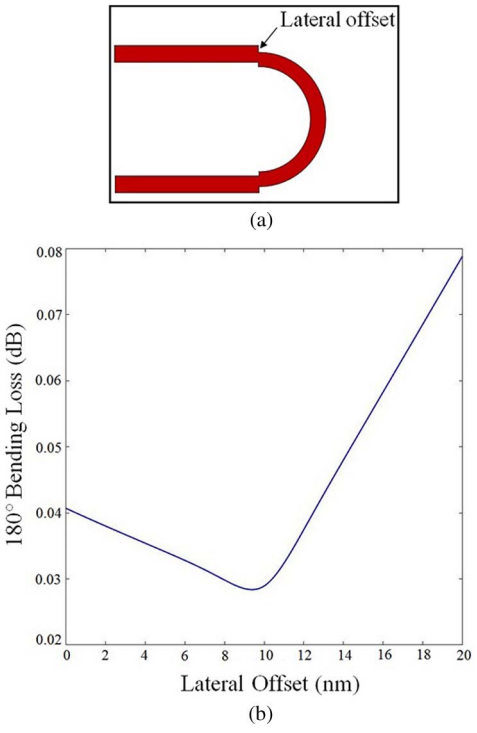

Fig. 3. (a) A top view of the 180° waveguide bend with a lateral offset. (b) 180° bending loss of a silicon waveguide as a function of the lateral offset. The width and thickness of the waveguide are 400 and 215.5 nm, respectively. The bend radius is 4.5 μm.

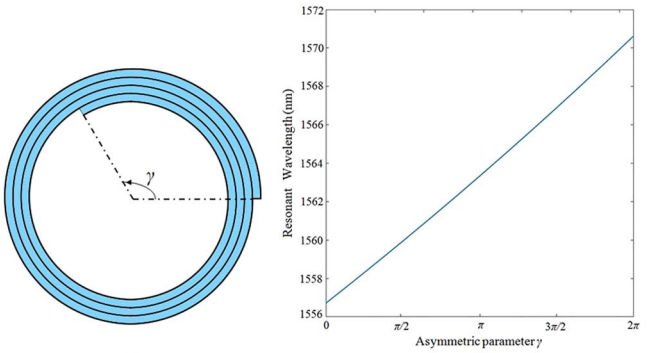

Fig. 4. (a) Non-scaled cross section of the free-standing part of the SRM, showing the inner edge, the outer edge, and the asymmetric parameter. (b) The resonant wavelength of the TiO_2 SRM as a function of the asymmetric parameter for the 65th azimuthal mode and the first radial mode. The design parameters are: SRM radius = 8 μm, winding number = 3, and bilayer thickness = 115 nm.

length of the traveling wave in the SRM and, consequently, raises the resonant wavelength from 1556.72 to 1570.62 nm. The simulation implies that designing the free-standing part of the SRM with a parabolic lobe-like pattern along the tube's axial direction enables us to extract different wavelengths from one SRM simultaneously.

The cross section of the OADM design as an SRM-based filter with $\gamma = 87.7°$ is demonstrated in Fig. 5. The SRM add–drop filter consists of unidirectional coupling between the free-standing part of the SRM and the input–output waveguides. In this configuration, the straight waveguides, which are placed close to the SRM along the axial direction, are introduced as the input–through and add–drop ports.

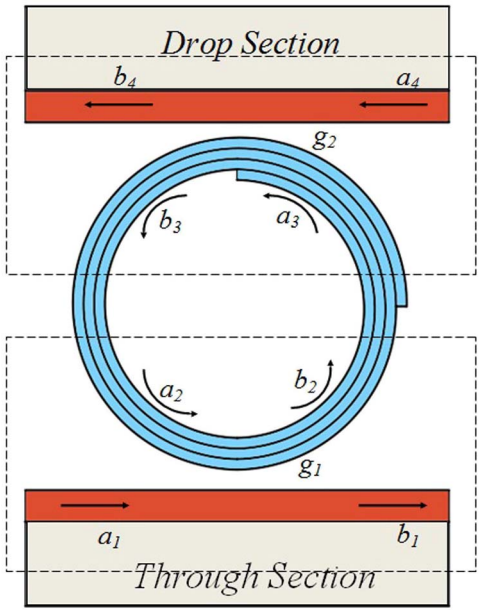

Fig. 5. Cross section of the two-channel OADM in the x–z plane at $\gamma = 87.7°$, which is composed of a free-standing part of a TiO_2 SRM coupled to the two straight waveguides embedded in two vertically aligned substrates.

The gaps between the SRM and each straight waveguide deposited on the substrates are assumed to be equal ($g_1 = g_2$). It should be noted that the mode profiles and coupling coefficients are computed by the 3D finite-difference time domain (FDTD) as an accurate numerical simulation method[19]. The coupled mode theory (CMT) is used to describe the filter transmission behavior[20]. Thus, the following relations are obtained:

$$b_1 = ta_1 - ika_2, \tag{1a}$$

$$b_2 = ta_2 - ika_1, \tag{1b}$$

$$b_3 = ta_3 - ika_4, \tag{1c}$$

$$b_4 = ta_4 - ika_3, \tag{1d}$$

$$a_4 = 0, \tag{1e}$$

where a_1, a_2 and b_1, b_2 are the input and output fields of the straight waveguide and the SRM in the through section, and a_3, a_4 and b_3, b_4 are the input and output fields of the SRM and the straight waveguide in the drop section, respectively, as shown in Fig. 5. t and k are the amplitude self- and cross-coupling coefficients. These formulas are derived by assuming a lossless coupling, where $t^2 + k^2 = 1$. It should be noted that the relative position of the edge of the SRM to the waveguide influences the fields of the SRM, self-, and cross-coupling coefficients.

The relationship between the SRM fields in the through and drop sections can be expressed as[20]

$$\begin{bmatrix} a_3 \\ b_3 \end{bmatrix} = \begin{bmatrix} 0 & e^{-i\tilde{\beta}\pi R} \\ e^{i\tilde{\beta}\pi R} & 0 \end{bmatrix} \begin{bmatrix} a_2 \\ b_2 \end{bmatrix}. \tag{2}$$

In the above definition, R is the effective radius of the SRM, and $\tilde{\beta} = \beta + i\alpha$, where β is the propagation constant of the fundamental mode in the SRM, and α is the loss coefficient in the SRM. It should be noted that R and $\tilde{\beta}$ are solved by the radial wave equation for an asymmetric SRM[17].

The resultant transfer function, representing the transmitted field in the drop port, is simplified to

$$T_{\text{drop}} = \frac{b_4}{a_1} = k^2 t^2 e^{-i\tilde{\beta}\pi R}\left(\frac{t}{t^2 - e^{i2\tilde{\beta}\pi R}} - 1\right). \tag{3}$$

Figure 6 shows the effect of g_1 on the transmittance coefficient ($20 \log |T_{\text{drop}}|$) at $\lambda = 1550.12$ nm. It can be found that the transmittance coefficient reaches the maximum value at $g_1 \cong 60$ nm. This value is selected in our design.

The performance of the proposed OADM can be explored from two perspectives: an optical demultiplexer and an optical multiplexer. The designated parameters are the ones that were discussed previously, and the waveguides are placed close to the free-standing part of the SRM along the axial direction at $\gamma = 87.7°$ and $\gamma = 76°$.

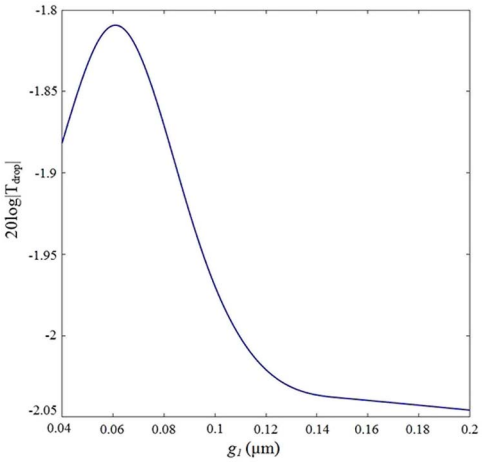

Fig. 6. Transmittance coefficient in the drop port as a function of the gap between the SRM and silicon waveguides.

Also, in order to have efficient coupling, the gap between the free-standing part of the SRM and the waveguides is adjusted to be 60 nm. Therefore, two different wavelengths (1548.52 nm at $\gamma = 76°$, 1550.12 nm at $\gamma = 87.7°$) in the C-band can be dropped or added simultaneously.

When the device serves as an optical demultiplexer, the SRM gets a broadband light (including $\lambda_1 \ldots \lambda_i \ldots \lambda_j \ldots \lambda_n$ wavelengths) from the input port, then drops the specific wavelengths (i.e., λ_i, λ_j) from the input ray according to the properties of the SRM along the axial direction to its drop ports, and finally sends the rest of the input wavelengths ($\lambda_1 \ldots \lambda_{i-1} \lambda_{i+1} \ldots \lambda_{j-1} \lambda_{j+1} \ldots \lambda_n$) to the through port. The drop ports spectra are depicted in Fig. 7.

The wavelengths of 1548.52 and 1550.12 nm are dropped at the ports 1 and 2, respectively. The free spectral range (FSR) of the device is about 20 nm. The adjacent channel spacing is 1.6 nm. The insertion losses for the drop ports 1 and 2 are 1.94 and 3.75 dB, respectively. The average 3 dB bandwidth is 1.8 nm. The adjacent channel crosstalk for the drop ports 1 and 2 are −9.1 and −6.036 dB, respectively.

When the OADM serves as an optical multiplexer, the broadband light is coupled to one of the add ports as an input. Figure 8 shows the spectral response at the drop ports when the signals are coupled into the add ports 1 and 2. The adjacent channel spacing is about 1.6 nm. As can be seen, when the add port 1/add port 2 acts as an input, the adjacent channel's crosstalk for the drop port 1/drop port 2 is $-11.9/-15.4$ dB. Moreover, the minimum insertion loss is about zero, which conveys that the added signals do not travel through the SRM, and the transmission loss in the SRM is excluded from the insertion loss. Excellent correspondence between the add and drop performance is observed. Hence, the proposed design can be considered as a perfectly efficient system for adding and dropping signals.

In conclusion, we propose a novel and compact layout for a two-channel OADM based on an SRM. In this scheme, the vertical integration of a 180° waveguide bend with a 4.5 μm bending radius and a single SRM having a parabolic lobe-like pattern in the axial direction allows us to efficiently add–drop two different wavelengths simultaneously. The simulations represent that tailoring the gap between the SRM and silicon waveguide affects the transmitted field in the drop port, which, consequently, results in an optimum gap of 60 nm. Furthermore, the performance of this design shows that the channel spacing is 1.6 nm, where any change in the asymmetric parameter tunes this characteristic as well as the minimum insertion loss value of 1.94 dB.

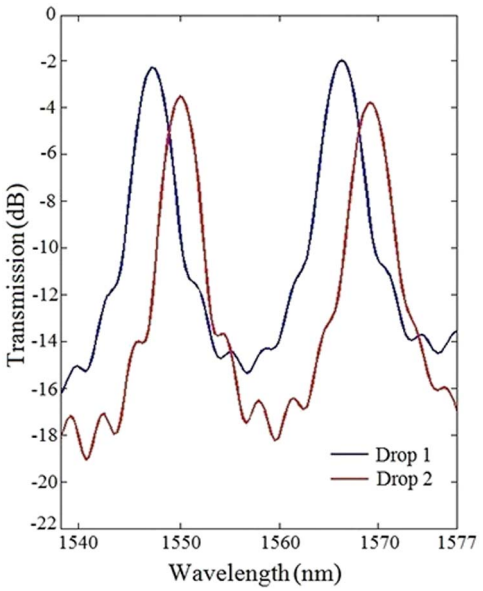

Fig. 7. Transmission spectra of the drop ports of the OADM when it serves as an optical demultiplexer.

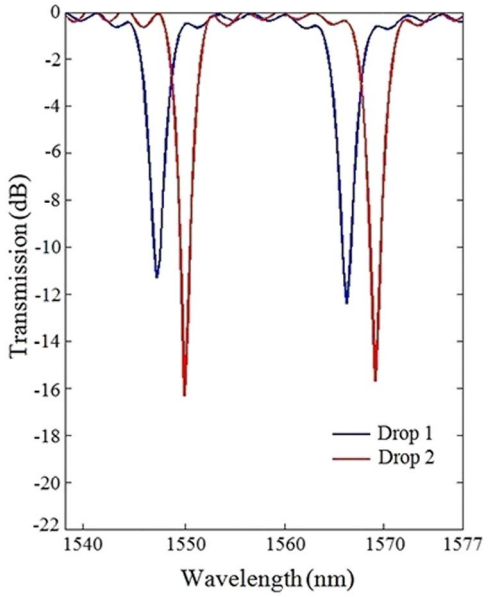

Fig. 8. Transmission spectra of "adds to drops" when it serves as an optical multiplexer.

References

1. Y. G. Han, S. B. Lee, C. S. Kim, and M. Y. Jeong, Opt. Lett. **31**, 703 (2006).
2. Y. Chu and H. Zhang, Chin. Opt. Lett. **1**, 196 (2003).
3. J. Wang and L. R. Chen, Opt. Express **23**, 26450 (2015).
4. H. Yan, X. Feng, D. Zhang, K. Cui, F. Liu, and Y. Huang, IEEE Photon. Technol. Lett. **25**, 1462 (2013).
5. D. Wu, Y. Wu, Y. Wang, J. An, and X. Hu, Opt Commun. **367**, 44 (2016).
6. J. T. Bessette and D. Ahn, Opt. Express **21**, 13580 (2013).
7. C. Strelow, C. M. Schultz, H. Rehberg, H. Welsch, C. Heyn, D. Heitmann, and T. Kipp, Phys. Rev. A **76**, 045303 (2007).
8. R. Songmuang, A. Rastelli, S. Mendach, and O. G. Schmidt, Appl. Phys. Lett. **90**, 091905 (2007).
9. C. Strelow, H. Rehberg, C. M. Schultz, H. Welsch, C. Heyn, D. Heitmann, and T. Kipp, Phys. Rev. Lett. **101**, 127403 (2008).
10. Q. Zhong, Z. Tian, M. H. Tavakoli Dastjerdi, Z. Mi, and D. V. Plant, Opt. Express **21**, 18909 (2013).
11. S. Böttner, S. Li, M. R. Jorgensen, and O. G. Schmidt, Appl. Phys. Lett. **102**, 251119 (2013).
12. A. Madani, M. Kleinert, D. Stolarek, L. Zimmermann, L. Ma, and O. G. Schmidt, Opt. Lett. **40**, 3826 (2015).
13. A. Liu, N. Izhaky, and L. Liao, in *Silicon Photonics: The State of the Art* (Wiley, 2008).
14. A. Madani, S. Böttner, M. R. Jorgensen, and O. G. Schmidt, Opt. Lett. **39**, 189 (2014).
15. A. Madani, L. Ma, S. Miao, M. R. Jorgensen, and O. G. Schmidt, Nanoscale **8**, 9498 (2016).
16. Y. Fang, S. Li, and Y. Mei, Phys. Rev. A **94**, 033804 (2016).
17. S. Sedaghat and A. Zarifkar, Opt. Commun. **382**, 167 (2017).
18. Y. Lan, S. Li, Z. Cai, Y. Mei, and S. Kiravittaya, Opt. Commun. **386**, 72 (2017).
19. C. Strelow, C. M. Schultz, H. Rehberg, M. Sauer, H. Welsch, A. Stemmann, C. Heyn, D. Heitmann, and T. Kipp, Phys. Rev. B **85**, 155329 (2012).
20. J. K. Poon, J. Scheuer, S. Mookherjea, G. T. Paloczi, Y. Huang, and A. Yariv, Opt. Express **12**, 90 (2004).